Macromolecules

Article

pubs.acs.org/Macromolecules

Effect of Induction on the Dispersion of Semiconducting and Metallic Single-Walled Carbon Nanotubes Using Conjugated Polymers

Nicole A. Rice, Ayyagari V. Subrahmanyam, Brian R. Coleman, and Alex Adronov*

Department of Chemistry, McMaster University, Hamilton, Ontario L8S 4L8, Canada

Supporting Information

ABSTRACT: Despite significant advances in single-walled carbon nanotube (SWNT) synthesis and purification strategies, the separation of metallic and semiconducting SWNTs on a large scale remains a barrier to the realization of many commercial applications. Selective extraction of specific SWNT types by wrapping and dispersion with conjugated polymers has been found effective for semiconducting SWNTs, but structural parameters that dictate selectivity are poorly understood. Here, we report nanotube dispersions with two structurally similar conjugated copolymers, both being poly(fluorene-*co*-phenylene) derivatives, having comparable degrees of polymerization but differing in the extent of electron donation from functional groups on the phenylene comonomers. It is found that copolymers decorated with electron donating methoxy functionalities lead to predominant dispersion of semiconducting SWNTs, while copolymers decorated with electron withdrawing nitro functionalities bias the dispersion toward metallic SWNTs. Differentiation of semiconducting and metallic SWNT populations was carried out by a combination of UV−vis−NIR absorption spectroscopy, Raman spectroscopy using multiple excitation wavelengths, and fluorescence spectroscopy. These results provide new insight into polymer design features that dictate preferential dispersion of specific SWNT types.

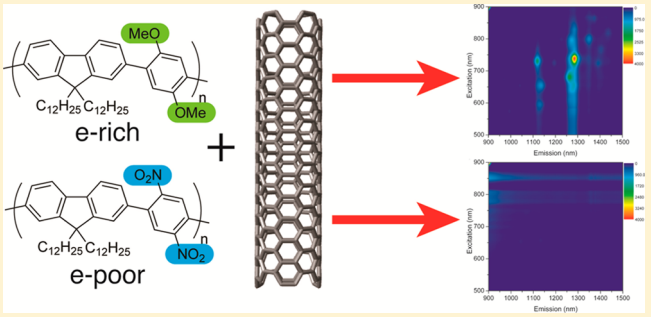

INTRODUCTION

Among the known nanoscale materials, single-walled carbon nanotubes (SWNTs) have attracted a tremendous amount of research attention since their discovery.[1−5] Their unique properties, including high tensile strength,[6] high aspect ratio,[7] thermal and electrical conductivity,[8−11] and extraordinary optical characteristics,[12−14] make them potentially valuable components of advanced materials with a wide range of applications. Indeed, SWNTs have been incorporated in field-effect transistors (FETs),[7,15] sensors,[16−19] photodetectors,[20] photovoltaics,[21−23] flexible printed circuits,[24] electrode materials for flexible electronics,[25] touch screens,[26] and microelectronic interconnects,[27] among other devices.[28] In these applications, the molecular nature, resilience, and amenity to chemical modification of SWNTs make them decisively advantageous over many other nanoscale materials. However, despite recent progress in nanotube commercialization,[27] applications that require controlled electrical and optical properties have not kept pace with expectations. This lag is a consequence of the inability to industrially prepare SWNTs that are pure in terms of their electrical properties. All known SWNT synthesis methods, such as high-pressure carbon monoxide disproportionation (HiPCO),[29] carbon vapor deposition (CVD),[30] arc discharge,[31] laser ablation,[32] and plasma torch growth,[33] result in the production of mixtures of metallic SWNTs (m-SWNTs) and semiconducting SWNTs (sc-SWNTs).[34] Since components of electronic devices require either m-SWNTs (electrodes, interconnects, etc.) or sc-SWNTs (transistors, sensors, etc.), their separation into pure samples is imperative. Several methods for separating and purifying SWNTs have recently been developed, including density-gradient ultracentrifugation (DGU),[35] agarose gel filtration,[36] electrophoresis,[37] and selective dispersion using conjugated polymers.[38] Of these, selective dispersion with conjugated polymers is promising as it is a low-cost and scalable process. While it has recently been shown that some conjugated polymers, such as commercially available polyfluorenes, can selectively disperse sc-SWNTs in toluene, the resulting dispersions are extremely dilute, precluding isolation of bulk quantities of purified SWNTs.[38] More importantly, selectivity for metallic SWNTs has not been reported and remains an elusive goal.

The selectivity of the interaction between conjugated polymers and SWNTs arises from a complex mixture of polymer features, including polymer structure, conformation, molecular weight, and the nature of the side chains.[39,40] Modification of some or all of these parameters has been demonstrated to have significant impact on the stability and selectivity of SWNT dispersions.[41,42] In addition to the polyfluorenes mentioned above, interactions of SWNTs with

Received: March 25, 2015
Revised: July 8, 2015

DOI: 10.1021/acs.macromol.5b00631
Macromolecules XXXX, XXX, XXX−XXX

Scheme 1. Synthesis of Monomers

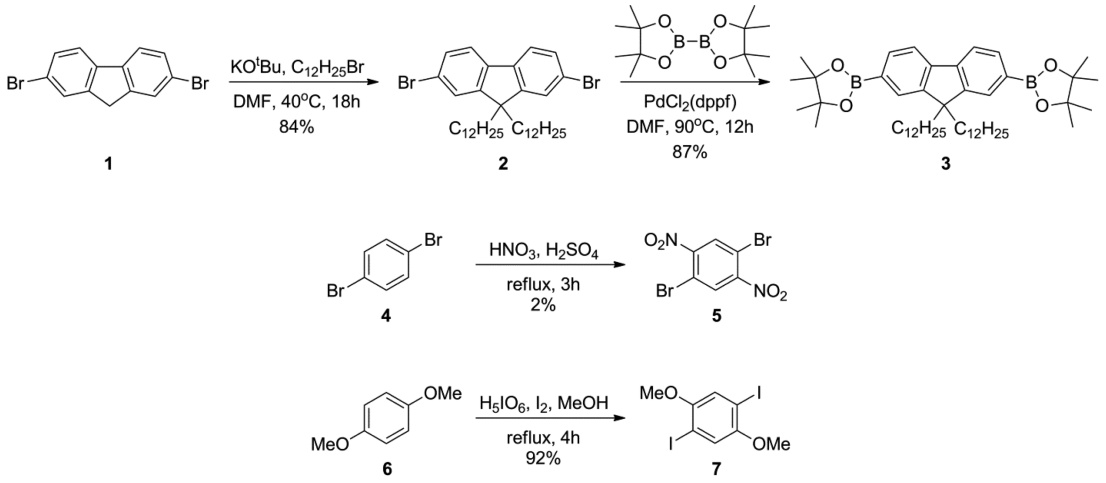

polythiophenes,[43] polycarbazoles,[44] poly(phenylenevinylene)s,[45] poly(phenyl acetylenes),[46] and a number of other structures and derivatives have been investigated.[47] Some of these structures have shown significant selectivity in their interactions with specific chiralities, diameters, and conductivity types, rivaling that of polyfluorenes. Despite this progress, a fundamental understanding of the interaction selectivity, from the perspective of controllable polymer characteristics such as backbone structure, side-chain structure, and electronic properties, has been elusive. One of the difficulties in determining the effect of structural variability on interaction selectivity is the fact that changing monomer structure often affects polymerization kinetics, solubility, and overall reactivity toward polymerization catalysts, which results in significant variability in the polymer chain length. It has been well documented that chain length, in addition to other structural elements, can have a significant impact on the types of SWNTs being dispersed by a particular polymer.[48,49] Thus, maintaining constant chain length is imperative when comparing polymers of different structure in their ability to disperse SWNTs, as this decreases the chance of inaccurate interpretation of observations.

In this report, we investigate how inductive effects of polymer side chains impact the electronic types of SWNTs that are dispersed by conjugated polymers composed of fluorene and phenylene units. We demonstrate that when other variables (such as molecular weight and size of side chains) are kept constant, the electronic nature of the polymer backbone has a significant effect on which species of SWNTs are dispersed. In particular, we observe that by changing from a simple electron-rich comonomer (*p*-dimethoxyphenyl) to an electron-poor comonomer (*p*-dinitrophenyl), it is possible to switch from dispersing solely sc-SWNTs to dispersing a mixture that contains significant amounts of m-SWNTs.

RESULTS AND DISCUSSION

Polymer Design and Synthesis. The polymer structures were carefully designed in an effort to minimize the various parameters that can affect the nature of the polymer−SWNT interaction and prevent unambiguous investigation of the effect of changing the electronic character of the conjugated polymer backbone on the polymer's ability to disperse SWNTs. In particular, polymer architecture has been shown to play an important role in the types of SWNTs that are dispersed[50−52] as well as on the stability of the polymer−SWNT complexes obtained.[53] Drastic changes in the size of the functionalities on the polymer backbone could change how the polymer wraps the SWNT surface, potentially interfering with the polymer−nanotube interaction. It was therefore desirable to keep side-chain size identical between different polymer structures. It was also important to obtain polymers with the same degree of polymerization, as polymer length has been previously demonstrated to significantly affect the quality of SWNT dispersions.[48,49]

A fluorene-containing polymer backbone was chosen because polyfluorenes have been shown to interact well with SWNTs and can exhibit selectivity toward small subsets of SWNTs under appropriate solvent conditions.[54] 1,4-Dibromo-2,5-dinitrobenzene and 1,4-diiodo-2,5-dimethoxybenzene were chosen as comonomers to produce the electron-poor and electron-rich polymer structures, respectively. The nitro and methoxy functionalities are comparable in size, allowing the two polymers to adopt similar conformations on the surface of SWNTs. The choice of small electronically inductive functionalities also avoids any negative steric interactions that could arise from the presence of bulky or drastically different side chains. Synthesis of the 9,9-bis(dodecyl)fluorene-2,7-diboronate ester monomer[55] (**3**) and the two comonomers, 1,4-dibromo-2,5-dinitrobenzene[56] (**5**) and 1,4-diiodo-2,5-dimethoxybenzene[57] (**7**), was accomplished according to literature procedures (Scheme 1).

The two poly(fluorene-*co*-phenylene) copolymers were prepared using Suzuki polycondensation conditions by reacting the 9,9-bis(dodecyl)fluorene-2,7-diboronate ester (**3**) with the corresponding electron-deficient and electron-rich monomers (**5** and **7**, respectively), as shown in Scheme 2. The nitro-containing copolymer (PFdNB) was prepared using PEPPSI-IPr[58] as the catalyst in a toluene/$K_2CO_{3(aq)}$ (2.5:1 v/v) cosolvent mixture. The crude polymer was purified by precipitation in methanol, followed by Soxhlet extraction in hexanes and acetone to yield a yellow solid in 81% yield. Gel permeation chromatography (GPC) indicated that the polymer had a number-average molecular weight (M_n) of 26.0 kDa, corresponding to a degree of polymerization (DP) of 39 repeat units (Table 1). The electron-rich methoxy-containing copolymer (PFdOMB) was prepared using a $Pd(PPh_3)_4$ catalyst in a DMF/toluene (3:1 v/v) cosolvent mixture. The PFdOMB polymer was also precipitated into methanol and purified using Soxhlet extraction with hexanes and acetone and

DOI: 10.1021/acs.macromol.5b00631
Macromolecules XXXX, XXX, XXX−XXX

Scheme 2. Synthesis of PFdNB and PFdOMB Copolymers by Suzuki Polycondensation

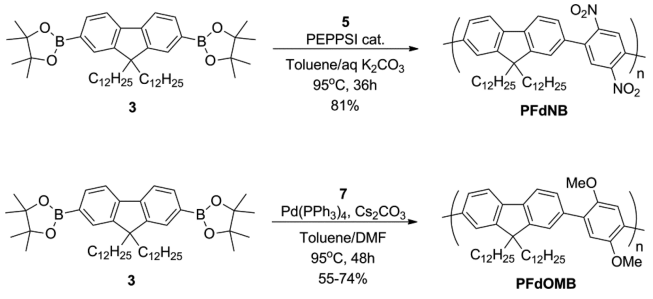

Table 1. Yield and Molecular Weight Data for Dinitro (PFdNB) and Dimethoxy (PFdOMB) Copolymers

polymer	yield (%)	M_n (kDa)	M_w (kDa)	PDI	DP[a]
PFdNB	81	26.0	49.8	1.92	39
$PFdOMB_{21}$	74	20.7	54.5	2.64	32
$PFdOMB_{27}$	55	26.9	59.2	2.20	42
$PFdOMB_{60}$	62	59.8	196.6	3.29	94

[a]Calculated from M_n values.

was isolated as a pale yellow solid. Several polymerization attempts were necessary to produce a polymer with M_n similar enough to PFdNB to allow for a valid comparison. The polymer fraction with the closest molecular weight to PFdNB had an M_n of 26.9 kDa ($PFdOMB_{27}$), which corresponds to a DP of 42 (Table 1). Two other polymerizations yielded significant amounts of the dimethoxy polymer, one with a slightly lower molecular weight ($PFdOMB_{21}$, M_n = 20.7 kDa) and one with a much higher molecular weight ($PFdOMB_{60}$, M_n = 59.8 kDa). These polymers were also used to prepare complexes with SWNTs (see Supporting Information) to investigate the effect of molecular weight on selectivity toward specific SWNT types. All the polymers used in this study exhibited excellent solubility in various organic solvents at room temperature, including THF, toluene, dichloromethane, and chloroform.

Polymer–SWNT Complexes. Supramolecular polymer–SWNT complexes were prepared using the different copolymers and raw HiPCO SWNTs following previously reported procedures.[59] Briefly, 5 mg of SWNTs was added to a polymer solution consisting of 10 mg of polymer dissolved in 20 mL of solvent. The mixture was sonicated for 1 h in a bath sonicator chilled with ice, followed by centrifugation at 8346*g* for 30 min. The supernatant was carefully removed from the centrifuge tube, filtered, and continuously washed with solvent to remove excess polymer. After removal of excess polymer, the polymer–SWNT buckypaper was redispersed in 15 mL of solvent by sonication, followed by a second centrifugation. A SWNT suspension using sodium dodecylbenzenesulfonate (SDBS) as the surfactant for nanotube dispersion was also prepared following literature procedures and used for comparison.[60]

Two different solvents, THF and toluene, were used in the initial studies. Consistent with previous results using poly(9,9-dioctylfluorene) (PFO),[60] we obtained relatively concentrated SWNT suspensions in THF using PFdNB–SWNT and the three PFdOMB–SWNT samples; however, with the exception of $PFdOMB_{60}$, these samples showed very little selectivity in the chiralities dispersed. In toluene, greater selectivity toward a smaller subset of chiralities was obtained, but this occurred at the expense of overall SWNT concentration.[60] A convenient compromise was found with a 1:1 THF/toluene (v/v) cosolvent mixture. This solvent system displayed almost identical selectivity results to those obtained in neat toluene, but with a concentration of SWNTs that was comparable to what is achieved in THF. In addition, nanotube suspensions remained stable for at least several months in this mixed solvent system, showing no difference in stability relative to either of the single solvents. This cosolvent mixture was used for all polymer–SWNT samples except $PFdOMB_{60}$–SWNT, for which THF was found to yield the best results. The $PFdOMB_{21}$–, $PFdOMB_{27}$–, and $PFdOMB_{60}$–SWNT samples were all clear, green dispersions, while the PFdNB–SWNT suspension exhibited an orange-brown color (see Supporting Information, Figure S3).

Polymer–SWNT Complex Characterization. To investigate the degree of nanotube bundling that is present in samples of the polymer-dispersed SWNTs, atomic force microscopy (AFM) studies were performed. Polymer–SWNT complex samples were prepared by spin-coating dilute dispersions on freshly cleaved mica. Tapping-mode AFM analysis was performed on these samples, and representative images from these studies are shown in Figure 1. Long,

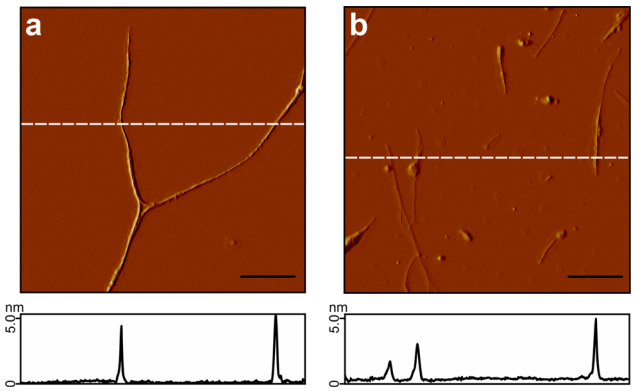

Figure 1. Representative AFM images for (a) $PFdOMB_{27}$–SWNT and (b) PFdNB–SWNT, with corresponding height profiles shown below. The dashed white lines represent the location of the height profile, and the black scale bars correspond to 500 nm.

filamentous structures were observed in both samples, with heights ranging from 1 to 5 nm. The smallest diameter features correspond to individual polymer-coated SWNTs, while the larger diameter features could arise from small polymer–SWNT bundles, which were either present in the dispersions or formed upon removal of the solvent during the spin-coating process. These observed height profiles indicate that significant exfoliation of nanotube bundles occurred upon sonication with both polymer types, and there was no appreciable difference in the degree of nanotube exfoliation by PFdOMB and PFdNB.

UV–vis–NIR absorption spectroscopy was performed on the polymer–SWNT supramolecular complexes (Figure 2). The absorption features for SWNTs arise from the interband transitions of the van Hove singularities, with different chiralities of SWNTs having different transition energies between the various allowed levels, enabling the electronic transitions to be organized as a function of diameter and chirality.[61] The absorbance features can be grouped into three categories in the observed absorbance range: two semiconducting regions, S_{11} (830–1600 nm) and S_{22} (600–800

DOI: 10.1021/acs.macromol.5b00631
Macromolecules XXXX, XXX, XXX–XXX

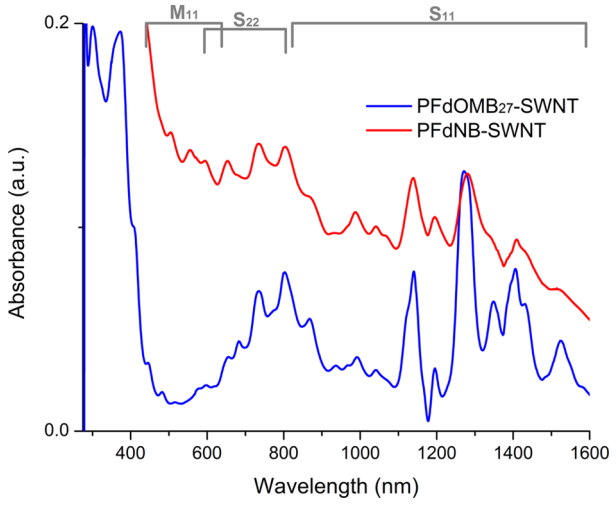

Figure 2. UV−vis−NIR absorption spectra for PFdOMB$_{27}$−SWNT (blue) and PFdNB−SWNT (red) in a 1:1 mixture of THF/toluene.

nm), and a metallic M_{11} (440−645 nm) region.[62] Despite spectral congestion in these regions, qualitative assignment based on peak location and shape can be made for the PFdOMB$_{27}$−SWNT complex in the S_{11} region (see Supporting Information, Table S1).

The absorption spectrum for PFdOMB$_{27}$−SWNT displays multiple intense, sharp features in both the S_{11} and S_{22} regions. This absorption spectrum suggests that the electron-rich PFdOMB effectively exfoliates sc-SWNTs in the THF/toluene cosolvent mixture. The location of the various peak maxima is red-shifted compared to a reference SDBS−SWNT dispersion (see Supporting Information, Figure S6), consistent with previous observations for conjugated polymer−SWNT supramolecular dispersions.[63] The PFdNB−SWNT absorption spectrum also contains multiple red-shifted peaks in the S_{11} and S_{22} regions; however, the peaks are broader and lack the fine features displayed by the PFdOMB$_{27}$−SWNT sample. The relatively intense, featureless absorption background of the PFdNB−SWNT spectrum is indicative of the presence of m-SWNTs.[64] However, detailed analysis of the M_{11} region is complicated for these samples as the polymer absorption overlaps in this region.

To further investigate the differences in nanotube populations dispersed by the two different polymers, resonance Raman spectroscopy was performed. This technique allows for identification of different SWNT species within a given sample as both m- and sc-SWNTs can be examined.[65] Resonance enhancement occurs when the excitation wavelength is tuned to overlap with the van Hove singularities present in the 1D density of states for a particular nanotube.[66] As these electronic transitions depend on nanotube diameter and chirality, only a subset of the total nanotube population will be enhanced and detected for any given excitation wavelength.[67] The low-frequency radial breathing mode (RBM, 100−400 cm^{-1}) is a particularly useful region for study as the peak locations have an inverse dependence on SWNT diameter.[68]

Thin film samples were prepared from the polymer−SWNT complexes by drop-casting the solutions onto silicon wafers and allowing the solvent to evaporate. A reference SWNT sample was also prepared by sonicating a small amount of the SWNT starting material in $CHCl_3$ and using this suspension to prepare a solid film using the same drop-casting method. Raman scans were obtained at three excitation wavelengths, including 514, 633, and 785 nm. It has previously been shown that these three excitation wavelengths are adequate for characterizing the electronic nature of a HiPCO SWNT sample, as both metallic and semiconducting species can be separately probed.[69] Figure 3 shows the RBM regions from the three samples at each excitation wavelength (full-scale Raman scans are provided in the Supporting Information, Figure S5). All Raman spectra were normalized to the G band at approximately 1590 cm^{-1} and offset for clarity. Upon excitation at 514 nm, two dominant RBM features are observed in the SWNT spectrum (Figure 3a, black curve): a broad feature arising from sc-SWNTs centered at 180 cm^{-1}, and several sharp peaks from 225 to 290 cm^{-1}, which are attributed to m-SWNTs.[70] Both the semiconducting and metallic features remain present in the PFdNB-SWNT sample (Figure 3a, red curve), while PFdOMB$_{27}$−SWNT only shows a single peak in the sc-SWNT region (Figure 3a, blue curve), suggesting that m-SWNTs are not present in this sample. This fact is corroborated by analysis of the G band region at this excitation wavelength, which is shown in the inset in Figure 3a. The G band is composed of two peaks: a lower frequency G$^-$ and a higher frequency G$^+$. For sc-SWNTs, both the G$^-$ and G$^+$ have Lorentzian line shapes, but for m-SWNTs the G$^-$ exhibits a broader Breit−Wigner−Fano (BWF) line shape.[71] A very broad G$^-$ band is observed for both the SWNT and PFdNB−SWNT samples but not for PFdOMB$_{27}$−SWNT, confirming that m-SWNTs are largely absent in the latter sample.

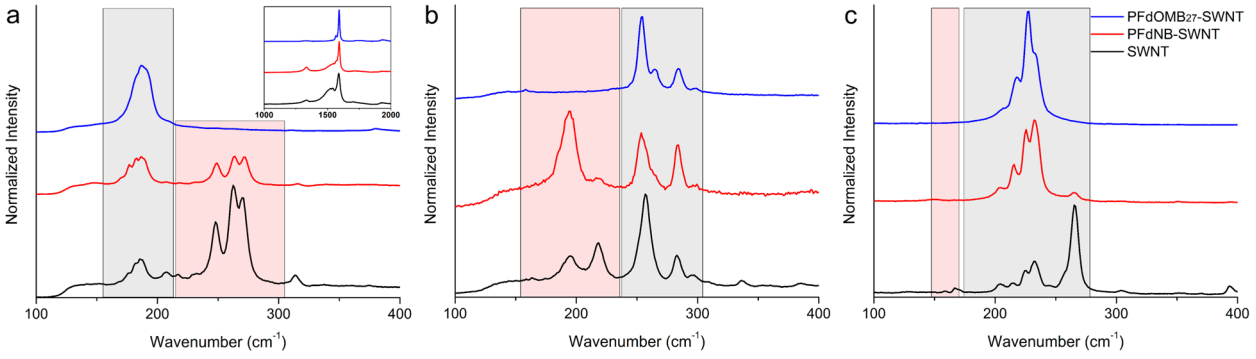

Figure 3. RBM regions of the Raman spectra using (a) 514, (b) 633, and (c) 785 nm excitation wavelengths. The gray regions represent locations of signals arising from semiconducting nanotubes, while the pink regions represent the locations of signals from metallic nanotubes. The inset in (a) shows the G-band region, located at ∼1590 cm^{-1}, upon excitation at 514 nm.

DOI: 10.1021/acs.macromol.5b00631
Macromolecules XXXX, XXX, XXX−XXX

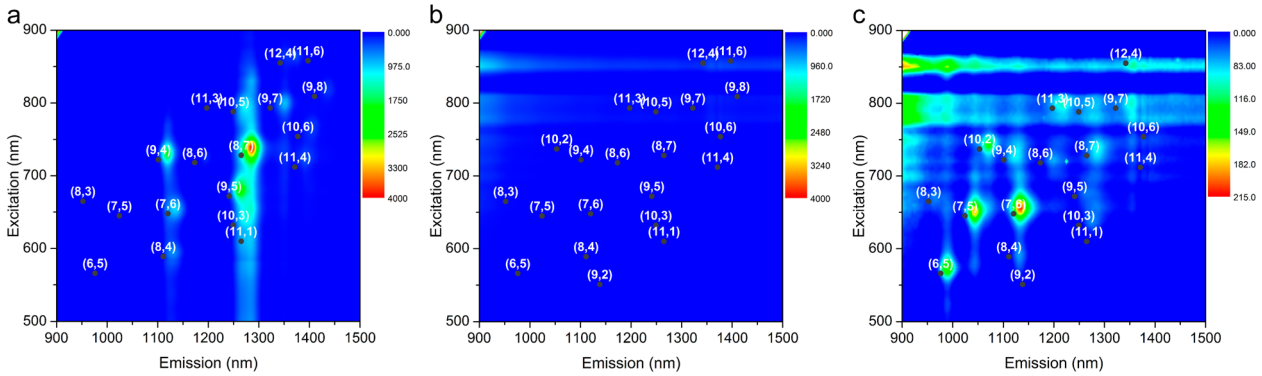

Figure 4. Photoluminescence maps (a) and (b) corresponding to PFdOMB$_{27}$–SWNT and PFdNB–SWNT at a similar concentration and plotted on the same scale. (c) is a more concentrated sample of PFdNB–SWNT, with the scale adjusted to show weak fluorescence.

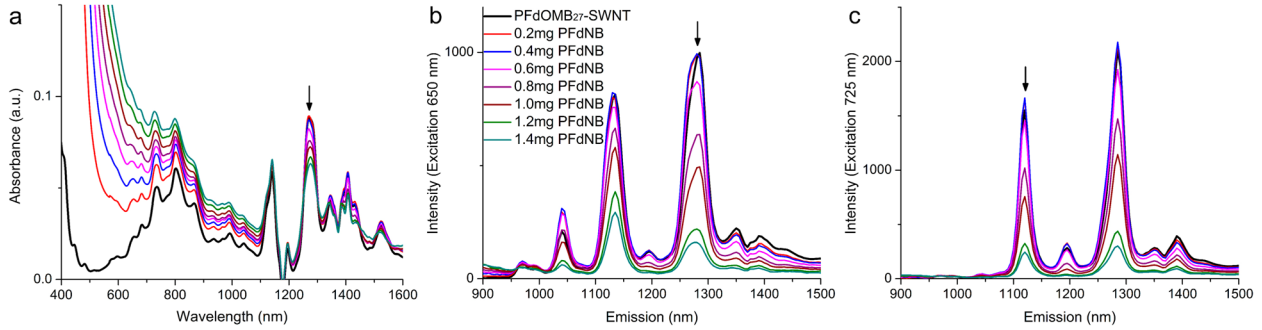

Figure 5. Absorption spectra (a) and PL spectra recorded using λ_{ex} = 650 (b) and 725 nm (c) upon addition of 50 μL aliquots of a 2 mg/mL solution of PFdNB to PFdOMB$_{27}$–SWNT. Plotted spectra represent samples after every second aliquot for clarity.

Both m- and sc-SWNTs are also in resonance when the 633 nm excitation wavelength is used. For HiPCO nanotube samples at this excitation wavelength, m-SWNT features are found at approximately 175–230 cm^{-1}, while sc-SWNTs give rise to peaks at approximately 230–300 cm^{-1}.[62,72] Both m- and sc-SWNT features are observed in the SWNT and PFdNB–SWNT samples, while only sc-SWNT features are observed for PFdOMB$_{27}$–SWNT, confirming the interpretation of results from 514 nm excitation.

While mainly semiconducting HiPCO SWNTs are in resonance with the 785 nm excitation wavelength, it has been reported that a few large diameter metallic species, most notably the (16, 7) and (12, 9) chiralities, may be observed in the low-frequency region.[68,70] Several small peaks were observed in the SWNT and PFdNB–SWNT spectra from 149 to 168 cm^{-1} and were assigned to m-SWNTs, while no features were observed below 200 cm^{-1} for the PFdOMB$_{27}$–SWNT sample (Figure 3c). The most intense peak in the SWNT spectrum occurs at 265 cm^{-1}, which arises from (10, 2) SWNTs that come into resonance with this excitation wavelength when they are bundled.[73] This peak is often referred to as the "bundling peak" and can be a useful handle to qualitatively identify the presence of bundling in a SWNT sample treated with various dispersants.[74] Figure 3c shows that a significant decrease in the bundling peak occurs when SWNTs are dispersed with PFdNB, suggesting that nanotube bundles are being efficiently exfoliated by this polymer. Furthermore, there is no peak present at 265 cm^{-1} for the PFdOMB$_{27}$–SWNT sample, which indicates either that the SWNTs are completely debundled or that the (10,2) chirality is not dispersed by PFdOMB$_{27}$ (see Figure 4a). On the basis of these results, it is clear that PFdOMB$_{27}$ disperses only sc-SWNTs, while PFdNB disperses a higher proportion of m-SWNTs, along with some amount of sc-SWNTs. In addition, we found that the two higher molecular-weight electron-rich polymers, PFdOMB$_{27}$ and PFdOMB$_{60}$, exhibit higher selectivity for sc-SWNTs relative to the lower molecular weight PFdOMB$_{21}$ (complete Raman analysis of these samples is provided in the Supporting Information, Figure S10 and preceding paragraphs).

Photoluminescence (PL) Mapping. PL maps were recorded for the polymer–SWNT samples (Figure 4) as well as for the SDBS–SWNT suspension (Supporting Information, Figure S6). The locations of the various SWNT fluorescence maxima were assigned according to previously published data.[13] High-intensity PL signals were observed for the PFdOMB$_{27}$–SWNT sample, with the most intense peak arising from the (8, 7) chirality (consistent with the major UV–vis–NIR absorption peak at 1287 nm, Figure 2). Both the PL map and absorption spectrum for PFdOMB$_{27}$–SWNT also show removal of some smaller diameter semiconducting species, such as the (6, 5) and (7, 5) chiralities. Additionally, intense PL signals were observed for the PFdOMB$_{21}$–SWNT and PFdOMB$_{60}$–SWNT dispersions (Supporting Information, Figure S11), but a slightly different distribution of chiralities was found. Overall, the PL and absorption spectra for all three PFdOMB–SWNT dispersions showed intense signals that can be mainly attributed to the (8, 7) chirality along with significant amounts of the (9, 4) and (7, 6) nanotube species.

The PL map for the PFdNB–SWNT sample is strikingly different. We initially recorded the map with a sample concentration that was very similar to that of PFdOMB$_{27}$–SWNT, by matching the absorption intensity for the (8, 7) chirality at 1287 nm (see Figure 2). Despite evidence from the

DOI: 10.1021/acs.macromol.5b00631
Macromolecules XXXX, XXX, XXX–XXX

absorption and Raman spectra for the presence of sc-SWNTs in the PFdNB−SWNT sample, the PL map did not display any fluorescence peaks of significant intensity (Figure 4b). After repeated attempts at various concentrations, a low-intensity PL map (Figure 4c) was recorded, with weak fluorescence from some low diameter SWNTs, such as (6, 5), (7, 5), and (7, 6), and very weak PL intensity from the (8, 7) chirality. Since m-SWNTs do not exhibit fluorescence,[75] and are known to quench the fluorescence of sc-SWNTs,[76] this result, in combination with the Raman data, indicates that PFdNB is much more selective for m-SWNTs than PFdOMB.

To further support the selectivity of PFdNB for m-SWNTs, it is necessary to rule out the possibility that the electron-poor polymer itself is responsible for quenching nanotube fluorescence. We therefore performed a polymer exchange experiment to ascertain whether quenching by the polymer was possible. A 2 mg/mL solution of PFdNB in the THF/toluene cosolvent mixture was prepared and added to a dilute sample of the $PFdOMB_{27}$−SWNT dispersion in small aliquots (50 μL increments, corresponding to 0.1 mg of PFdNB). The sample was sonicated for 10 min after each addition, and an absorption and two PL spectra (at λ_{ex} = 650 and 725 nm) were recorded. The results of this experiment (Figure 5a−c) show an increase in the absorption intensity from 600 to 1100 nm, attributed to the tail end of the PFdNB polymer absorbance (which is present in large excess). Initially, as the PFdNB polymer was added there was no change in the SWNT PL intensity. However, upon the sixth addition a slight decrease in the PL intensity was noticed for both excitation wavelengths. A continual decrease in PL intensity was observed upon addition of subsequent aliquots. However, this decrease is attributed to the dilution of SWNTs, rather than to quenching, as a similar decrease in SWNT PL intensity was observed in a control experiment where identical volumes of pure solvent were added to the same starting concentration of $PFdOMB_{27}$−SWNT (see Supporting Information, Figure S7).

CONCLUSIONS

In the design of next-generation polymers for selective dispersion and purification of SWNTs, it is imperative to understand the key parameters that dictate polymer selectivity toward specific SWNT types. We have demonstrated that modification of the poly(fluorene-*co*-phenylene) backbone with electron-donating or electron-withdrawing functionalities can have a significant impact on the electronic nature of the SWNTs dispersed by the polymer. The copolymer bearing electron-donating methoxy functional groups interacts preferentially with semiconducting SWNTs, while the nearly identical copolymer bearing electron-withdrawing nitro functionalities produces dispersions that are much more enriched in metallic SWNTs (though some semiconducting SWNTs are still present). Considering that the fluorene unit is relatively electron rich itself, and preferentially interacts with semiconducting SWNTs, it is not surprising that exclusive dispersion of metallic SWNTs was not achieved in this case. Nevertheless, the electron-rich copolymer shows a clear preference for semiconducting SWNTs, while the electron-poor copolymer shows a bias toward metallic SWNTs. This work justifies further investigation of more electron-poor conjugated polymers for their ability to exhibit greater selectivity for metallic SWNTs.

ASSOCIATED CONTENT

Supporting Information

Full experimental details, full characterization of the polymers, photographs of polymer−SWNT dispersions, spectral data for an SDBS-dispersed SWNT reference sample, details of quenching studies, and spectral data for $PFdOMB_{21}$−SWNT and $PFdOMB_{60}$−SWNT samples. The Supporting Information is available free of charge on the ACS Publications website at DOI: 10.1021/acs.macromol.5b00631.

AUTHOR INFORMATION

Corresponding Author

*E-mail adronov@mcmaster.ca; Tel (905) 525-9140 x23514; Fax (905) 521-2773 (A.A.).

Notes

The authors declare no competing financial interest.

ACKNOWLEDGMENTS

Financial support for this work was provided by the National Science and Engineering Research Council of Canada (NSERC) and the Canada Foundation for Innovation (CFI). N. Rice is grateful for support through an NSERC-PGS scholarship.

REFERENCES

(1) Iijima, S.; Ichihashi, T. *Nature* **1993**, *363*, 603−605.
(2) Ajayan, P. M. *Chem. Rev.* **1999**, *99*, 1787−1800.
(3) *Carbon Nanotubes and Related Structures: Synthesis, Characterization, Functionalization, and Applications*; Guldi, D. M., Martín, N., Eds.; Wiley-VCH: Weinheim, 2010.
(4) Harris, P. J. F. *Carbon Nanotube Science: Synthesis, Properties and Applications*; Cambridge University Press: Cambridge, 2009.
(5) Saito, R.; Dresselhaus, M. S.; Dresselhaus, G. *Physical Properties of Carbon Nanotubes*; Imperial College Press: London, 1998.
(6) Yu, M.-F.; Files, B. S.; Arepalli, S.; Ruoff, R. S. *Phys. Rev. Lett.* **2000**, *84*, 5552−5555.
(7) Terrones, M. *Annu. Rev. Mater. Res.* **2003**, *33*, 419−501.
(8) Han, Z.; Fina, A. *Prog. Polym. Sci.* **2011**, *36*, 914−944.
(9) Avouris, P.; Chen, Z.; Perebeinos, V. *Nat. Nanotechnol.* **2007**, *2*, 605−615.
(10) Avouris, P. *Acc. Chem. Res.* **2002**, *35*, 1026−1034.
(11) Collins, P. G.; Avouris, P. *Sci. Am.* **2000**, *283*, 62−69.
(12) O'Connell, M. J.; Bachilo, S. M.; Huffman, C. B.; Moore, V. C.; Strano, M. S.; Haroz, E. H.; Rialon, K. L.; Boul, P. J.; Noon, W. H.; Kittrell, C.; Ma, J.; Hauge, R. H.; Weisman, R. B.; Smalley, R. E. *Science* **2002**, *297*, 593−596.
(13) Weisman, R. B.; Bachilo, S. M. *Nano Lett.* **2003**, *3*, 1235−1238.
(14) Kataura, H.; Kumazawa, Y.; Maniwa, Y.; Umezu, I.; Suzuki, S.; Ohtsuka, Y.; Achiba, Y. *Synth. Met.* **1999**, *103*, 2555−2558.
(15) Durkop, T.; Getty, S. A.; Cobas, E.; Fuhrer, M. S. *Nano Lett.* **2004**, *4*, 35−39.
(16) Qi, P.; Vermesh, O.; Grecu, M.; Javey, A.; Wang, Q.; Dai, H.; Peng, S.; Cho, K. J. *Nano Lett.* **2003**, *3*, 347−351.
(17) Dionisio, M.; Schnorr, J. M.; Michaelis, V. K.; Griffin, R. G.; Swager, T. M.; Dalcanale, E. *J. Am. Chem. Soc.* **2012**, *134*, 6540−6543.
(18) Rivas, G. A.; Rubianes, M. D.; Rodriguez, M. C.; Ferreyra, N. F.; Luque, G. L.; Pedano, M. L.; Miscoria, S. A.; Parrado, C. *Talanta* **2007**, *74*, 291−307.
(19) Pang, X.; Imin, P.; Zhitomirsky, I.; Adronov, A. *Macromolecules* **2010**, *43*, 10376−10381.
(20) Nanot, S.; Hároz, E. H.; Kim, J.-H.; Hauge, R. H.; Kono, J. *Adv. Mater.* **2012**, *24*, 4977−4994.
(21) Rowell, M. W.; Topinka, M. A.; McGehee, M. D.; Prall, H.-J.; Dennler, G.; Sariciftci, N. S.; Hu, L.; Grüner, G. *Appl. Phys. Lett.* **2006**, *88*, 233506.

DOI: 10.1021/acs.macromol.5b00631
Macromolecules XXXX, XXX, XXX−XXX

(22) Bindl, D. J.; Safron, N. S.; Arnold, M. S. *ACS Nano* **2010**, *4*, 5657−5664.
(23) Keru, G.; Ndungu, P. G.; Nyamori, V. O. *Int. J. Energy Res.* **2014**, *38*, 1635−1653.
(24) Sun, D.-M.; Liu, C.; Ren, W.-C.; Cheng, H.-M. *Small* **2013**, *9*, 1188−1205.
(25) Green, A. A.; Hersam, M. C. *Nano Lett.* **2008**, *8*, 1417−1422.
(26) Hecht, D. S.; Thomas, D.; Hu, L.; Ladous, C.; Lam, T.; Park, Y.; Irvin, G.; Drzaic, P. *J. Soc. Inf. Dispersion* **2009**, *17*, 941−946.
(27) De Volder, M. F. L.; Tawfick, S. H.; Baughman, R. H.; Hart, A. J. *Science* **2013**, *339*, 535−539.
(28) Jariwala, D.; Sangwan, V. K.; Lauhon, L. J.; Marks, T. J.; Hersam, M. C. *Chem. Soc. Rev.* **2013**, *42*, 2824−2860.
(29) Nikolaev, P.; Bronikowski, M. J.; Bradley, R. K.; Rohmund, F.; Colbert, D. T.; Smith, K. A.; Smalley, R. E. *Chem. Phys. Lett.* **1999**, *313*, 91−97.
(30) Kong, J.; Cassell, A. M.; Dai, H. J. *Chem. Phys. Lett.* **1998**, *292*, 567−574.
(31) Journet, C.; Maser, W. K.; Bernier, P.; Loiseau, A.; Lamy de la Chapelle, M.; Lefrant, S.; Deniard, P.; Lee, R.; Fischer, J. E. *Nature* **1997**, *388*, 756−758.
(32) Guo, T.; Nikolaev, P.; Thess, A.; Colbert, D. T.; Smalley, R. E. *Chem. Phys. Lett.* **1995**, *243*, 49−54.
(33) Kim, K. S.; Cota-Sanchez, G.; Kingston, C. T.; Imris, M.; Simard, B.; Soucy, G. *J. Phys. D: Appl. Phys.* **2007**, *40*, 2375−2387.
(34) Rafique, M. M. A.; Iqbal, J. *J. Encapsulation Adsorpt. Sci.* **2011**, *1*, 29−34.
(35) Arnold, M. S.; Green, A. A.; Hulvat, J. F.; Stupp, S. I.; Hersam, M. C. *Nat. Nanotechnol.* **2006**, *1*, 60−65.
(36) Liu, H.; Feng, Y.; Tanaka, T.; Urabe, Y.; Kataura, H. *J. Phys. Chem. C* **2010**, *114*, 9270−9276.
(37) Tanaka, T.; Jin, H.; Miyata, Y.; Kataura, H. *Appl. Phys. Express* **2008**, *1*, 114001.
(38) Nish, A.; Hwang, J.-Y.; Doig, J.; Nicholas, R. J. *Nat. Nanotechnol.* **2007**, *2*, 640−646.
(39) Gao, J.; Kwak, M.; Wildeman, J.; Herrmann, A.; Loi, M. A. *Carbon* **2011**, *49*, 333−338.
(40) Berton, N.; Lemasson, F.; Hennrich, F.; Kappes, M. M.; Mayor, M. *Chem. Commun.* **2012**, *48*, 2516−2518.
(41) Lemasson, F.; Berton, N.; Tittmann, J.; Hennrich, F.; Kappes, M. M.; Mayor, M. *Macromolecules* **2012**, *45*, 713−722.
(42) Berton, N.; Lemasson, F.; Tittmann, J.; Stürzl, N.; Hennrich, F.; Kappes, M. M.; Mayor, M. *Chem. Mater.* **2011**, *23*, 2237−2249.
(43) Lee, H. W.; Yoon, Y.; Park, S.; Oh, J. H.; Hong, S.; Liyanage, L. S.; Wang, H.; Morishita, S.; Patil, N.; Park, Y. J.; Park, J. J.; Spakowitz, A.; Galli, G.; Gygi, F.; Wong, P. H. S.; Tok, J. B.-H.; Kim, J. M.; Bao, Z. *Nat. Commun.* **2011**, *2*, 541−548.
(44) Lemasson, F. A.; Strunk, T.; Gerstel, P.; Hennrich, F.; Lebedkin, S.; Barner-Kowollik, C.; Wenzel, W.; Kappes, M. M.; Mayor, M. *J. Am. Chem. Soc.* **2011**, *133*, 652−655.
(45) Keogh, S. M.; Hedderman, T. G.; Gregan, E.; Farrell, G.; Chambers, G.; Byrne, H. J. *J. Phys. Chem. B* **2004**, *108*, 6233−6241.
(46) Liang, S.; Chen, G.; Peddle, J.; Zhao, Y. *Chem. Commun.* **2012**, *48*, 3100−3102.
(47) Tuncel, D. D. *Nanoscale* **2011**, *3*, 3545−3554.
(48) Imin, P.; Cheng, F.; Adronov, A. *Polym. Chem.* **2011**, *2*, 1404−1408.
(49) Jakubka, F.; Schießl, S. P.; Martin, S.; Englert, J. M.; Hauke, F.; Hirsch, A.; Zaumseil, J. *ACS Macro Lett.* **2012**, *1*, 815−819.
(50) Gao, J.; Loi, M. A.; de Carvalho, E. J. F.; dos Santos, M. C. *ACS Nano* **2011**, *5*, 3993−3999.
(51) Akazaki, K.; Toshimitsu, F.; Ozawa, H.; Fujigaya, T.; Nakashima, N. *J. Am. Chem. Soc.* **2012**, *134*, 12700−12707.
(52) Ozawa, H. H.; Fujigaya, T. T.; Niidome, Y. Y.; Hotta, N. N.; Fujiki, M. M.; Nakashima, N. N. *J. Am. Chem. Soc.* **2011**, *133*, 2651−2657.
(53) Liu, J.; Moo-Young, J.; McInnis, M.; Pasquinelli, M. A.; Zhai, L. *Macromolecules* **2014**, *47*, 705−712.
(54) Ding, J.; Li, Z.; Lefebvre, J.; Cheng, F.; Dubey, G.; Zou, S.; Finnie, P.; Hrdina, A.; Scoles, L.; Lopinski, G. P.; Kingston, C. T.; Simard, B.; Malenfant, P. R. L. *Nanoscale* **2014**, *6*, 2328−2339.
(55) Jo, J.; Chi, C.; Höger, S.; Wegner, G.; Yoon, D. Y. *Chem. - Eur. J.* **2004**, *10*, 2681−2688.
(56) Jackson, C. L.; Calhane, D. F. *Am. Chem. J.* **1902**, *28*, 451−474.
(57) Wariishi, K.; Morishima, S.; Inagaki, Y. *Org. Process Res. Dev.* **2003**, *7*, 98−100.
(58) O'Brien, C. J.; Kantchev, E. A. B.; Valente, C.; Hadei, N.; Chass, G. A.; Lough, A.; Hopkinson, A. C.; Organ, M. G. *Chem. - Eur. J.* **2006**, *12*, 4743−4748.
(59) Imin, P.; Imit, M.; Adronov, A. *Macromolecules* **2012**, *45*, 5045−5050.
(60) Hwang, J.-Y.; Nish, A.; Doig, J.; Douven, S.; Chen, C.-W.; Chen, L.-C.; Nicholas, R. J. *J. Am. Chem. Soc.* **2008**, *130*, 3543−3553.
(61) Bachilo, S. M.; Strano, M. S.; Kittrell, C.; Hauge, R. H.; Smalley, R. E.; Weisman, R. B. *Science* **2002**, *298*, 2361−2366.
(62) Strano, M. S.; Dyke, C. A.; Usrey, M. L.; Barone, P. W.; Allen, M. J.; Shan, H.; Kittrell, C.; Hauge, R. H.; Tour, J. M.; Smalley, R. E. *Science* **2003**, *301*, 1519−1522.
(63) Furmanchuk, A.; Leszczynski, J.; Tretiak, S.; Kilina, S. V. *J. Phys. Chem. C* **2012**, *116*, 6831−6840.
(64) Naumov, A. V.; Ghosh, S.; Tsyboulski, D. A.; Bachilo, S. M.; Weisman, R. B. *ACS Nano* **2011**, *5*, 1639−1648.
(65) Dresselhaus, M. S.; Jorio, A.; Hofmann, M.; Dresselhaus, G.; Saito, R. *Nano Lett.* **2010**, *10*, 751−758.
(66) Dresselhaus, M. S.; Dresselhaus, G.; Saito, R.; Jorio, A. *Phys. Rep.* **2005**, *409*, 47−99.
(67) Doorn, S. K. *J. Nanosci. Nanotechnol.* **2005**, *5*, 1023−1034.
(68) Doorn, S. K.; Heller, D. A.; Barone, P. W.; Usrey, M. L.; Strano, M. S. *Appl. Phys. A: Mater. Sci. Process.* **2004**, *78*, 1147−1155.
(69) Strano, M. S.; Zheng, M.; Jagota, A.; Onoa, G. B.; Heller, D. A.; Barone, P. W.; Usrey, M. L. *Nano Lett.* **2004**, *4*, 543−550.
(70) Strano, M. S.; Doorn, S. K.; Haroz, E. H.; Kittrell, C.; Hauge, R. H.; Smalley, R. E. *Nano Lett.* **2003**, *3*, 1091−1096.
(71) Brown, S. D. M.; Jorio, A.; Corio, P.; Dresselhaus, M. S.; Dresselhaus, G.; Saito, R.; Kneipp, K. *Phys. Rev. B: Condens. Matter Mater. Phys.* **2001**, *63*, 155414.
(72) Strano, M. S.; Zheng, M.; Jagota, A.; Onoa, G. B.; Heller, D. A.; Barone, P. W.; Usrey, M. L. *Nano Lett.* **2004**, *4*, 543−550.
(73) Heller, D. A.; Barone, P. W.; Swanson, J. P.; Mayrhofer, R. M.; Strano, M. S. *J. Phys. Chem. B* **2004**, *108*, 6905−6909.
(74) O'Connell, M. J.; Sivaram, S.; Doorn, S. K. *Phys. Rev. B: Condens. Matter Mater. Phys.* **2004**, *69*, 235415.
(75) Hároz, E. H.; Duque, J. G.; Tu, X.; Zheng, M.; Walker, A. R. H.; Hauge, R. H.; Doorn, S. K.; Kono, J. *Nanoscale* **2013**, *5*, 1411−1439.
(76) Zhang, D.; Yang, J.; Li, Y. *Small* **2013**, *9*, 1284−1304.

DOI: 10.1021/acs.macromol.5b00631
Macromolecules XXXX, XXX, XXX−XXX